



Skeletal mineralogy in a high-CO₂ world

Justin B. Ries*

Department of Marine Sciences, University of North Carolina - Chapel Hill, Chapel Hill, North Carolina 27599, USA

Department of Geology and Geophysics, Woods Hole Oceanographic Institution, Woods Hole, Massachusetts 02543, USA

ARTICLE INFO

Article history:

Received 21 March 2011

Received in revised form 8 April 2011

Accepted 9 April 2011

Available online 10 May 2011

Keywords:

Aragonite

Calcite

Mg-calcite

Mg-fractionation

Shell

Skeleton

ABSTRACT

Increasing atmospheric pCO₂ reduces the saturation state of seawater with respect to the aragonite, high-Mg calcite (Mg/Ca > 0.04), and low-Mg calcite (Mg/Ca < 0.04) minerals from which marine calcifiers build their shells and skeletons. Notably, these polymorphs of CaCO₃ have different solubilities in seawater: aragonite is more soluble than pure calcite, and the solubility of calcite increases with its Mg-content. Although much recent progress has been made investigating the effects of CO₂-induced ocean acidification on rates of biological calcification, considerable uncertainties remain regarding impacts on shell/skeletal polymorph mineralogy. To investigate this subject, eighteen species of marine calcifiers were reared for 60-days in seawater bubbled with air-CO₂ mixtures of 409 ± 6, 606 ± 7, 903 ± 12, and 2856 ± 54 ppm pCO₂, yielding aragonite saturation states (Ω_A) of 2.5 ± 0.4, 2.0 ± 0.4, 1.5 ± 0.3, and 0.7 ± 0.2. Calcite/aragonite ratios within biminerals calcifiers increased with increasing pCO₂, but were invariant within monomineralic calcifiers. Calcite Mg/Ca ratios (Mg/Ca_C) also varied with atmospheric pCO₂ for two of the five high-Mg-calcite-producing organisms, but not for the low-Mg-calcite-producing organisms. These results suggest that shell/skeletal mineralogy within some—but not all—marine calcifiers will change as atmospheric pCO₂ continues rising as a result of fossil fuel combustion and deforestation. Paleocceanographic reconstructions of seawater Mg/Ca, temperature, and salinity from the Mg/Ca_C of well-preserved calcitic marine fossils may also be improved by accounting for the effects of paleo-atmospheric pCO₂ on skeletal Mg-fractionation.

© 2011 Elsevier B.V. All rights reserved.

1. Introduction

Increasing atmospheric pCO₂ causes more CO₂ to dissolve in seawater, which reduces seawater pH, carbonate ion concentration ([CO₃²⁻]), and saturation state (Ω) with respect to the CaCO₃ minerals from which marine calcifiers build their shells and skeletons. However, the different forms or 'polymorphs' of CaCO₃ utilized by marine calcifiers have different solubilities in seawater: aragonite is more soluble than pure calcite, and the solubility of calcite increases with its Mg/Ca ratio (Fig. 1; Andersson et al., 2008). Thus, CO₂-induced ocean acidification could potentially alter the mineralogical composition and ultrastructure of the shells and skeletons that calcareous organisms evolved largely to protect themselves from predation (e.g., Vermeij, 1989).

Calcite/aragonite and Mg/Ca_C ratios within many species of marine calcifiers are known to vary as a function of various environmental parameters, including seawater Mg/Ca (reviewed by Ries, 2010) and temperature (Chave, 1954; Lowenstam, 1954)—indicating that shell/skeletal polymorph mineralogy within such organisms is a phenotypically plastic trait. Furthermore, recent laboratory experiments have revealed that the polymorph mineralogy of abiotically precip-

itated CaCO₃ varies as a function of CO₂-induced changes in the CaCO₃ saturation state of seawater (e.g., de Choudens-Sanchez and Gonzalez, 2009; Lee and Morse, 2010). Here, I present experiments that investigate whether CO₂-induced ocean acidification impacts the polymorph mineralogy of biologically precipitated carbonates—i.e., the shells and skeletons of marine calcifiers.

2. Methods

2.1. Overview of experimental design

To investigate the impact of CO₂-induced ocean acidification on the polymorph mineralogy and Mg/Ca_C of calcifying marine organisms, eighteen species—including six that produce predominantly (>97% of CaCO₃) aragonite (hard clam, soft clam, limpet, conch, calcareous green alga, coral), five that produce predominantly (>97% of CaCO₃) low-Mg calcite (periwinkle, bay scallop, oyster, blue mussel), six that produce predominantly (>97% of CaCO₃) high-Mg calcite (two species of urchin, coralline red algae, lobster, blue crab, shrimp), and two that produce relatively equitable mixtures of aragonite and calcite (serpulid worm, whelk)—were reared for 60 days in isothermal (25 °C) experimental seawaters continuously bubbled with mixed gases of 409 ± 6, 606 ± 7, 903 ± 12, and 2856 ± 54 ppm pCO₂ (± SD), which yielded average (± SD) Ω_A of 2.5 ± 0.4, 2.0 ± 0.4, 1.5 ± 0.3, and 0.7 ± 0.2 (Table 1). These Ω_A were selected to

* Tel.: +1 919 536 9070; fax: +1 919 962 1254.

E-mail address: riesjustin@gmail.com.

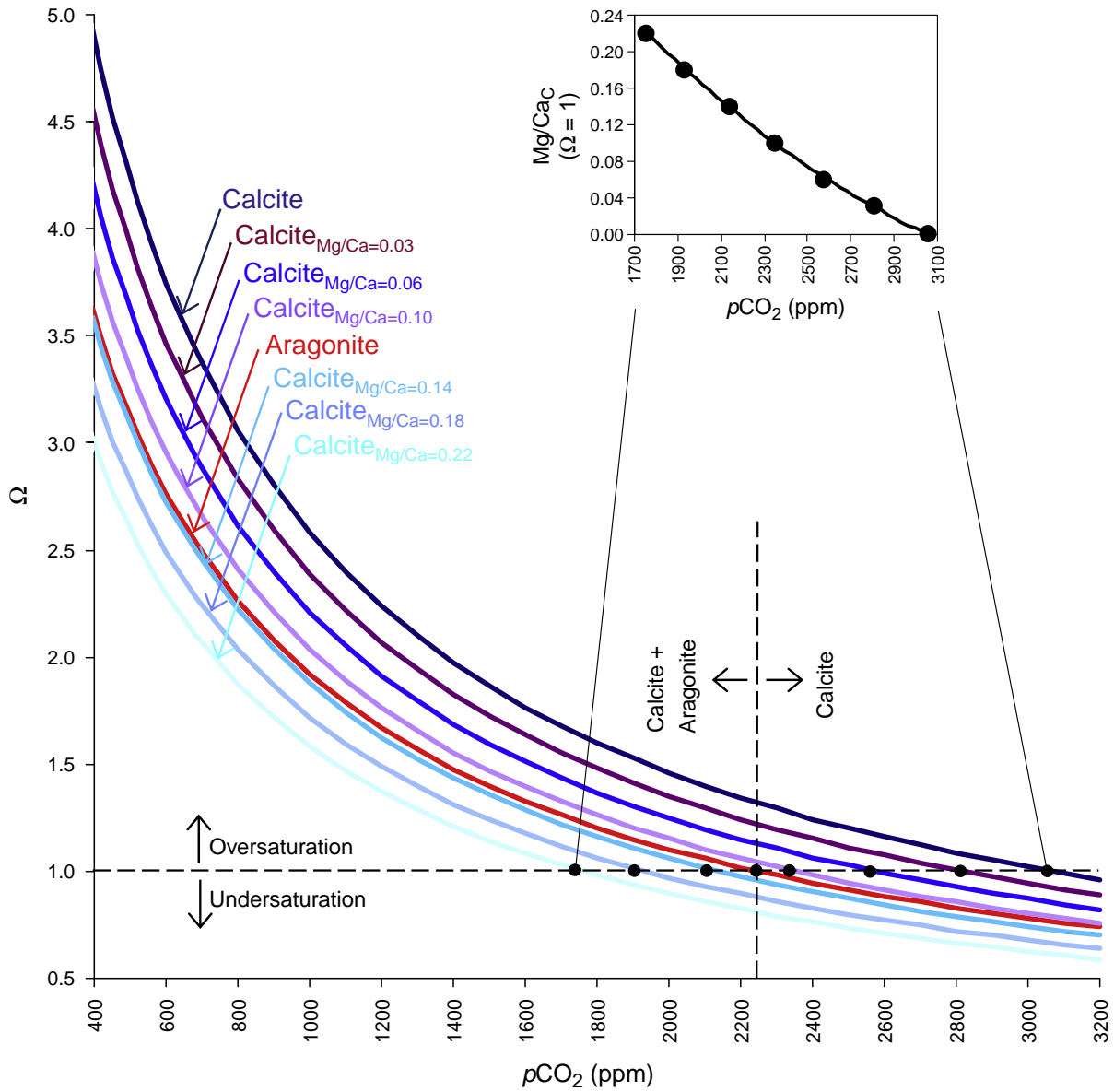


Fig. 1. Seawater saturation state (Ω) with respect to aragonite (red curve), calcite (dark blue), and biogenic Mg-calcites with Mg/Ca_C of 0.03, 0.06, 0.10, 0.14, 0.18, and 0.22 (various blue-purple curves) as a function of atmospheric pCO₂. The solubility of calcite increases with its Mg-content, such that the solubility of Mg-calcite with Mg/Ca_C = 0.14 is approximately equivalent to that of aragonite. At atmospheric pCO₂ between approximately 2250 and 3050 ppm, seawater is simultaneously oversaturated with respect to pure calcite yet undersaturated with respect to aragonite. Inset graph illustrates how the Mg/Ca_C of Mg-calcite in equilibrium with seawater ($\Omega = 1$) declines with increasing atmospheric pCO₂. These calculations form the theoretical basis for the hypothesis that marine calcifiers would begin producing lower Mg-calcite (i.e., a less soluble form of CaCO₃) instead of higher Mg-calcite and aragonite in response to increasing atmospheric pCO₂. Calculations assume instantaneous equilibrium between the atmosphere and the surface seawater, total alkalinity = 2300 $\mu\text{mol kg SW}^{-1}$, salinity = 35, and temperature = 25 °C. Seawater saturation states with respect to the biogenic Mg-calcites were calculated pursuant to the solubility curve of “cleaned” biogenic calcites (Bischoff et al., 1983). Modified from Andersson et al. (2008).

span values predicted for the next several centuries in both surface waters of the open ocean (e.g., Brewer, 1997) and in regions affected by the upwelling of more acidic waters (Feely et al., 2008).

2.2. Specimen collection

Organisms were collected, pursuant to local, state, and federal regulations, from the following US localities (Table 2): *Callinectes sapidus* (blue crab) from the Chesapeake Bay, Maryland; *Homarus americanus* (american lobster) from the Gulf of Maine; *Penaeus plebejus* (edible shrimp), *Eucidaris tribuloides* (pencil urchin) and *Arbacia punctulata* (purple urchin) from the Atlantic Ocean off the coast of Florida; *Littorina littorea* (periwinkle), *Urosalpinx cinerea* (whelk), *Crepidula fornicata* (limpet), *Mytilus edulis* (blue mussel),

and *Crassostrea virginica* (eastern oyster) from Buzzards Bay, Massachusetts; *Strombus alatus* (conch) from the Gulf of Mexico off the coast of Florida; *Hydroides crucigera* (feather duster worm), *Mercenaria mercenaria* (quahog), *Mya arenaria* (softshell clam), and *Argopecten irradians* (bay scallop) from Nantucket Sound off the coast of Massachusetts; and *Oculina arbuscula* (temperate coral) from the Atlantic Ocean off the coast of North Carolina. After collection, organisms were transported by airplane, boat, or automobile to the Environmental Systems Laboratory at the Woods Hole Oceanographic Institution, where they were immediately placed in holding tanks bubbled with ambient air (pCO₂ = 409 ppm ± 6). After approximately 14 days of acclimatization to the laboratory conditions, healthy specimens were transferred to the experimental seawaters for an additional 14 days of acclimatization prior to the official start of the experiment.

Table 1
Average measured and calculated carbonate system parameters of the experimental seawaters (from Ries et al., 2009).

	Measured parameters										Calculated parameters							
	pCO ₂ -g (ppm) ^a	SD ^b	Sal ^c	SD	Temp ^d (°C)	SD	Alk ^e (μM)	SD	pH	SD	DIC ^f (μM)	SD	pCO ₂ -e (ppm) ^g	SD	Ω _A ^h	SD	t-test ⁱ	P-value ^j
Crustacea aquaria (lobster/crab/ shrimp)	409	6	32.0	0.2	24.9	0.2	1860	157	8.03	0.06	1678	140	526	63	2.1	0.4	n/a	n/a
	606	7	31.8	0.1	25.0	0.1	1849	131	7.85	0.10	1732	119	839	171	1.5	0.4	2.5	0.02
	903	12	32.1	1.0	25.0	0.2	1817	162	7.72	0.06	1744	155	1146	124	1.1	0.2	1.9	0.05
	2856	54	31.9	0.2	25.1	0.1	1817	171	7.31	0.03	1860	169	3103	217	0.5	0.1	5.8	0.00
Mollusk aquaria (conch/limpet/whelk /periwinkle)	409	6	31.8	0.1	25.1	0.1	1770	108	8.09	0.03	1568	101	420	46	2.3	0.2	n/a	n/a
	606	7	31.8	0.2	24.9	0.2	1798	142	8.00	0.07	1634	147	561	137	1.9	0.3	2.4	0.02
	903	12	31.9	0.2	24.9	0.1	1849	63	7.86	0.07	1733	78	831	168	1.5	0.2	2.8	0.01
	2856	54	31.7	0.1	24.9	0.1	2079	124	7.42	0.07	2097	111	2758	316	0.7	0.1	8.0	0.00
Algae aquaria (coralline red alga/ halimeda)	409	6	31.8	0.2	25.0	0.1	2008	56	8.19	0.03	1738	50	359	32	3.1	0.2	n/a	n/a
	606	7	31.7	0.1	25.0	0.2	1987	127	8.05	0.06	1786	101	526	68	2.4	0.4	3.4	0.01
	903	12	31.5	0.2	25.1	0.2	2044	53	7.91	0.03	1903	46	802	48	1.8	0.1	2.8	0.02
	2856	54	31.8	0.3	24.9	0.1	2354	37	7.49	0.02	2350	33	2593	106	0.9	0.1	15.3	0.00
Echinoid aquaria (pencil urchin/purple urchin)	409	6	31.9	0.3	25.1	0.1	1744	147	8.04	0.06	1563	127	473	67	2.1	0.3	n/a	n/a
	606	7	31.8	0.1	25.0	0.2	1751	168	7.90	0.05	1623	145	686	35	1.6	0.3	2.4	0.02
	903	12	31.7	0.3	24.9	0.1	1792	117	7.77	0.02	1707	108	999	44	1.2	0.1	2.5	0.02
	2856	54	31.7	0.2	25.0	0.1	1891	78	7.36	0.03	1921	73	2854	159	0.5	0.1	10.0	0.00
Coral/serpulid worm aquaria	409	6	31.7	0.2	25.0	0.2	1960	30	8.11	0.06	1738	47	450	83	2.6	0.3	n/a	n/a
	606	7	31.6	0.4	24.9	0.1	2012	37	8.03	0.04	1824	32	573	52	2.3	0.2	2.0	0.05
	903	12	31.7	0.4	24.9	0.1	2027	30	7.85	0.05	1907	30	915	110	1.6	0.2	5.0	0.00
	2856	54	31.5	0.6	25.2	0.1	2071	48	7.48	0.03	2070	40	2377	128	0.8	0.1	9.0	0.00
Bivalve aquaria (clams/mussel/scallop/oyster)	409	6	32.1	0.3	25.1	0.1	1833	125	8.15	0.04	1598	112	370	46	2.6	0.3	n/a	n/a
	606	7	31.7	0.2	25.1	0.1	1862	141	8.02	0.08	1684	126	547	119	2.1	0.4	2.3	0.03
	903	12	31.9	0.3	25.0	0.2	1856	92	7.83	0.05	1749	87	892	108	1.4	0.2	3.5	0.01
	2856	54	31.9	0.2	25.0	0.1	2063	43	7.45	0.04	2071	51	2551	256	0.7	0.0	10.1	0.00

(a) 'pCO₂-g' = measured pCO₂ of gas bubbled into experimental seawaters.

(b) 'SD' = standard deviation.

(c) 'Sal' = salinity.

(d) 'Temp' = temperature.

(e) 'Alk' = total alkalinity (μmol/kg-SW).

(f) 'DIC' = dissolved inorganic carbon (μmol/kg-SW).

(g) 'pCO₂-e' = calculated pCO₂ of gas in equilibrium with experimental seawaters.

(h) 'Ω_A' = aragonite saturation state.

(i) 't-test' = student's t-test statistic.

(j) P-value ≤ 0.05 (denoted with bold font) indicates that Ω_A of a given experimental seawater is significantly less (at the 95% confidence level) than Ω_A of the experimental seawater bubbled with the next lowest pCO₂.

2.3. Culturing conditions

Organisms were reared in 24 38-liter glass aquaria filled with 0.2 μm-filtered seawater obtained from Great Harbor in Vineyard Sound off the coast of Cape Cod, Massachusetts. The aquaria were divided into six sets of four, with each set of four being exposed to the same suite of four mixed gases (409 ± 6, 606 ± 7, 903 ± 12, 2856 ± 54 ppm pCO₂). Similar and compatible organisms were grouped in the same sets of aquaria as follows: set 1 - *Callinectes sapidus* (blue crab), *Penaeus plebejus* (edible shrimp), and *Homarus americanus* (american lobster); set 2 - *Littorina littorea* (periwinkle), *Urosalpinx cinerea* (whelk), *Crepidula fornicata* (limpet), and *Strombus alatus* (conch); set 3 - *Halimeda incrassata* (calcareous green alga) and *Neogoniolithon* sp. (coralline alga); set 4 - *Eucidaris tribuloides* (tropical urchin) and *Arbacia punctulata* (temperate urchin); set 5 - *Hydroides crucigera* (feather duster worm) and *Oculina arbuscula* (temperate coral); and set 6 - *Mercenaria mercenaria* (quahog), *Mytilus edulis* (blue mussel), *Mya arenaria* (softshell clam), *Argopecten irradians* (bay scallop), and *Crassostrea virginica* (eastern oyster).

Less than 60 g of living biomass (wet-weight) was maintained in each experimental aquarium. Organic acids were removed from the experimental aquaria by the reactive carbon filtration system. Any build up of organic acids between water changes or throughout the duration of the experiment would have been detected by the weekly pH measurements and the biweekly alkalinity determinations, and thus accounted for in the calculations of CaCO₃ saturation state. However, no major changes in pH (SD < 0.10; Table 1) or alkalinity (SD < 171 μmol/kg-SW; Table 1) were detected throughout the experiment.

Heterotrophic organisms were fed every other day as follows: 900 mg wet-weight (w-wt) frozen brine shrimp to each *Callinectes sapidus* (blue crab) and *Homarus americanus* (american lobster); 210 mg w-wt edible shrimp to each *Penaeus plebejus* (edible shrimp); 10 mg dry-weight (d-wt) green algae to each *Littorina littorea* (periwinkle), *Urosalpinx cinerea* (whelk), *Crepidula fornicata* (limpet); 50 mg d-wt green algae to each *Strombus alatus* (conch); 90 mg d-wt green algae to each *Eucidaris tribuloides* (tropical urchin) and *Arbacia punctulata* (temperate urchin); 90 mg w-wt frozen brine shrimp to each *Hydroides crucigera* (feather duster worm); 330 mg w-wt frozen brine shrimp to each colony of *Oculina arbuscula* (temperate coral); 290 mg w-wt puréed frozen brine shrimp and 10 mg d-wt puréed green algae to each *Mercenaria mercenaria* (quahog), *Mytilus edulis* (blue mussel), *Mya arenaria* (softshell clam), *Argopecten irradians* (bay scallop), and *Crassostrea virginica* (eastern oyster).

The experimental seawaters were maintained at 25 ± 1 °C using 50-watt electric heaters. Each tank was continuously filtered with polyester fleece and activated carbon at the rate of 600 L/h. Aquaria housing the gastropods, the calcifying algae, and the corals/serpulid worms were illuminated with 10 hours/day of 426 W per square meter (W/m²) irradiance (T8, 8000 K aquarium spectrum lamps), aquaria housing the urchins and bivalves were illuminated with 10 hours/day of 213 W/m² irradiance (T8, 8000 K aquarium spectrum lamps), and aquaria housing the crustacea were not illuminated.

The experimental air-CO₂ gases were formulated using Cole-Parmer mass flow controllers (catalog #: K-32907-51; K-32661-16; 00119FB). These air-CO₂ gas mixtures were introduced to the aquaria with 6-inch micro-porous air-stones secured to the base of the aquaria at approximately 30 cm depth. Each aquarium and

Table 2

Scientific name, collection site, annual water temperature range, developmental stage, and portion of shell/skeleton analyzed for the investigated organisms.

Organism	Scientific name	Collection site	Ann temp range (°C) ^a	Age	Site of analysis
Lobster	<i>Homarus americanus</i>	Gulf of Maine, ME	1–26	juvenile	body carapace
Crab	<i>Callinectes sapidus</i>	Chesapeake Bay, MD	3–32	juvenile	body carapace
Shrimp	<i>Penaeus plebejus</i>	Atlantic Ocean, FL	20–32	adult	body carapace
Conch	<i>Strombus alatus</i>	Gulf of Mexico, FL	20–30	adult	distal edge
Limpet	<i>Crepidula fornicata</i>	Buzzards Bay, MA	3–28	adult	distal edge
Whelk	<i>Urosalpinx cinerea</i>	Buzzards Bay, MA	3–28	adult	distal edge
Periwinkle	<i>Littorina littorea</i>	Buzzards Bay, MA	3–28	adult	distal edge
Coralline alga	<i>Neogoniolithon</i> sp.	Atlantic Ocean, FL	20–32	adult	branch tip
Halimeda	<i>Halimeda incrassata</i>	Atlantic Ocean, FL	20–32	adult	newest segment
Pencil urchin	<i>Eucidaris tribuloides</i>	Atlantic Ocean, FL	20–32	adult	spine tip/coronal plate
Purple urchin	<i>Arbacia punctulata</i>	Nantucket Sound, MA	1–27	adult	spine tip/coronal plate
Coral	<i>Oculina arbuscula</i>	Atlantic Ocean, NC	15–30	adult	apical corallite
Serpulid worm	<i>Hydroides crucigera</i>	Nantucket Sound, MA	1–27	adult	tube opening
Hard clam	<i>Mercenaria mercenaria</i>	Nantucket Sound, MA	1–27	adult	distal edge
Blue mussel	<i>Mytilus edulis</i>	Buzzards Bay, MA	3–28	adult	distal edge
Soft clam	<i>Mya arenaria</i>	Nantucket Sound, MA	1–27	adult	distal edge
Bay scallop	<i>Argopecten irradians</i>	Nantucket Sound, MA	1–27	adult	distal edge
Oyster	<i>Crassostrea virginica</i>	Buzzards Bay, MA	3–28	adult	distal edge

(a) National Oceanic and Atmospheric Administration, 2008.

attached filtration system was covered with plastic wrap to facilitate equilibration between the gas mixtures and the experimental seawaters and to minimize evaporative water-loss. Seventy-five percent seawater changes, using seawater pre-equilibrated with the experimental air-CO₂ mixtures, were made approximately every 14 days.

2.4. Controlling for 'tank effects' and 'data clustering'

To control for potential 'tank-effects', specimens and the four mixed-gas lines were swapped amongst aquaria. Specimens were removed from their aquaria and temporarily placed in holding aquaria approximately midway through the experiment pre-conditioned with the appropriate mixed gases. The gas lines were then rotated and the experimental seawaters were allowed to re-equilibrate. After the replaced seawater had re-equilibrated with the new gas mixtures, specimens were rotated amongst the aquaria pursuant to the rotation of the mixed gases. So-called 'tank effects' should be minimized by exposing the specimens to different aquaria throughout the course of the experiment.

To control for potential 'data clustering' due to growth of different specimens within the same tank, statistical trends were assessed with Generalized Estimating Equations that utilize the Huber-White sandwich estimator of variance (also known as the 'Robust Covariance

Matrix') in place of the standard estimator of variance (Rogers, 1993). Essentially, instead of employing statistical parameters that assume that the data are normally distributed about the mean (via the standard estimator of variance), the Huber-White estimator of variance uses a Taylor Series Expansion to adjust the statistical parameters so that they are based on the actual distribution of the data in each of the tanks – thus subjecting the data to a more rigorous test for statistical significance.

2.5. ¹³⁷Ba/¹³⁸Ba isotope marker for identifying new shell/skeletal material

The start of calcification under the experimental conditions was marked in the specimens' shells or skeletons by a ¹³⁷Ba/¹³⁸Ba isotope spike that had been added to the experimental seawaters at the start of the experiment (Fig. 2). In brief, each 38-liter experimental seawater treatment was dosed with 0.49 mg ¹³⁷BaCO₃ for 14 days at the beginning of the 60-day experiment, which quintupled the concentration of ¹³⁷Ba in the experimental seawaters, while only increasing total Ba concentration by approximately 45%. This temporary increase in concentration of ¹³⁷Ba in the experimental seawaters at the start of the experiment resulted in an approximately five-fold spike in ¹³⁷Ba/¹³⁸Ba within the skeletons or shells of the organisms, which was located by scanning along the growth axis via laser ablation-inductively coupled plasma-mass spectrometry (ThermoFinnigan Element2 ICP-MS; NewWave 213 nm wavelength laser; beam diameter = 5 μm; scan speed = 6 μm/sec; intensity = 35%; frequency 8 Hz; see Ries et al., 2010, for detailed methods).

This spike was identified in the shells/skeletons of all specimens, revealing that the investigated organisms continued accreting new shell/skeletal material along zones of calcification under each of the experimental pCO₂ treatments, despite some of the aragonite-producing organisms losing shell/skeletal mass on a net basis under the highest pCO₂ treatment, apparently via dissolution of portions of their shell or skeleton distal to the zone of calcification (Ries et al., 2009). The location of the ¹³⁷Ba/¹³⁸Ba isotope spike was etched into the skeleton with the 213 nm laser to demarcate skeletal/shell material accreted exclusively under the experimental conditions.

2.6. Measurement of seawater parameters (Ries et al., 2009)

Temperature was measured with a NIST-certified partial-immersion mercury-glass thermometer (precision = ± 0.3%, accuracy = ± 0.4%). Salinity was determined from the measurement of total dissolved solids (TDS) and/or using a refractometer calibrated with simultaneous

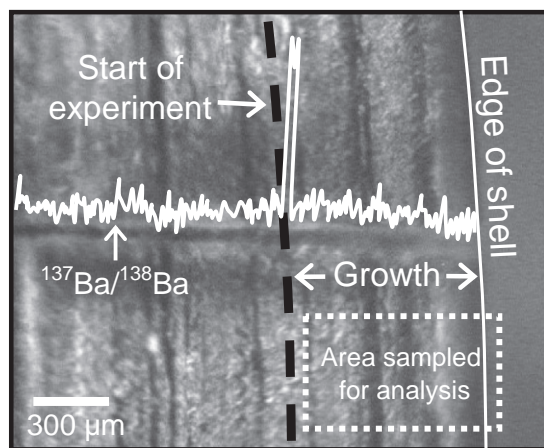


Fig. 2. ¹³⁷Ba/¹³⁸Ba profile of a *Mytilus edulis* shell that incorporated the ¹³⁷Ba spike at the start of the experiment, which was used to identify shell/skeletal material produced exclusively under the experimental conditions.

determinations of TDS (precision = $\pm 0.3\%$; accuracy = $\pm 0.4\%$). Seawater pH was determined weekly using an Orion pH electrode/meter calibrated with certified NBS pH buffers of 4.01, 7.00, and 10.01 (precision = ± 0.01 ; accuracy = ± 0.02). Total alkalinity of seawater in each aquarium was determined via small (precision = $\pm 0.5\%$, accuracy = $\pm 0.5\%$) and/or large volume Gran titrations (precision = $\pm 0.3\%$, accuracy = $\pm 0.3\%$) calibrated with certified Dickson seawater alkalinity standards. Mixed-gas pCO₂ was measured with a Qubit S151 infrared pCO₂ analyzer calibrated with certified air-CO₂ mixed-gas standards (precision = $\pm 2.0\%$; accuracy = $\pm 1.8\%$). Temperature, salinity, and pH of the experimental seawaters were measured weekly, while total alkalinity of the experimental seawaters and pCO₂ of the mixed gases were measured biweekly. Timing of seawater measurements was rotated between the beginning, middle, and end of the interval between water changes in order to capture changes in seawater parameters between water changes, as well as throughout the duration of the experiment.

The use of NBS buffers to calibrate the pH electrode introduces a systematic error arising from the difference in liquid junction potential of the electrode in the NBS buffers and in the experimental seawater solutions. However, dissolved inorganic carbon (DIC) calculated from simultaneous measurements of pH (calibrated with NBS buffers), total alkalinity, temperature, and salinity had an average %-difference of only 1.7% relative to DIC values determined independently by large volume Gran Titration (Bradshaw et al., 1981) calibrated with certified Dickson DIC standards (precision = $\pm 0.1\%$, accuracy = $\pm 0.1\%$; see Ries et al., 2009).

2.7. Calculation of carbonate system parameters (Ries et al., 2009)

Aragonite saturation state (Ω_A) and DIC of the experimental seawaters, and pCO₂ of the gas in equilibrium with the experimental seawaters (pCO₂-e), were calculated (Table 1) from the measured values of temperature, salinity, total alkalinity and pH using the program CO2SYS (Pierrot et al., 2006) with Roy et al. (1993) values for carbonic acid constants K_1^* and K_2^* , Mucci (1983) value for stoichiometric the stoichiometric aragonite solubility product, and pressure = 1.15 atm. Differences amongst Ω_A for the experimental seawaters equilibrated with the four pCO₂ levels are statistically significant ($p \leq 0.05$) for each of the six sets of aquaria (Table 1).

It should be noted that the total alkalinity in several sets of tanks was greater for treatments bubbled with the highest pCO₂ gas (2856 ppm) than for tanks bubbled with lower pCO₂ gases (409, 606, 903 ppm; Table 1). This was caused by the dissolution of CaCO₃ that occurred in response to the undersaturated conditions ($\Omega_A < 1$) within the highest pCO₂ treatments. This should not pose a problem for the interpretation of the results because the mineralogical responses are presented as a function of the saturation state of seawater with respect to aragonite (Ω_A). Since Ω_A is calculated from both the pH and total alkalinity of the seawater, should account for the effects of the increased alkalinity.

2.8. Determination of polymorph mineralogy

The %-calcite of CaCO₃, %-aragonite of CaCO₃ and Mg/Ca_c were determined via powder X-ray diffraction (XRD). Skeletal/shell material accreted exclusively under the experimental conditions was identified relative to the ¹³⁷Ba/¹³⁸Ba isotope marker emplaced in the shell/skeleton at the start of the experiment (see Section 2.5; Fig. 2) and then extracted under a stereomicroscope using a scalpel, tweezers, and a micromanipulator (see Table 2 for portion of shell/skeleton analyzed for each species).

Approximately 30 mg of newly accreted shell/skeletal material was mixed with 20 drops of 95% ethanol and gently ground for 30 s into a fine powder using an agate mortar and pestle. The slurry was injected into a 1 cm × 1 cm × 10 μm reservoir on a glass slide and

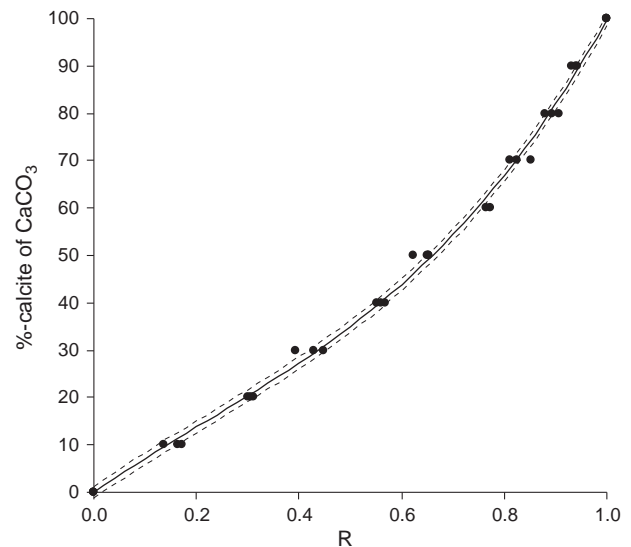


Fig. 3. Calibration curve relating %-calcite to the ratio (R) of the area under the primary calcite peak $d(104)$ to the sum of the area under the aragonite peaks $d(111)$ and $d(021)$ and the area under the primary calcite peak $d(104)$: %-calcite = $69.93761R^3 - 45.49681R^2 + 75.25000R$ (standard error of regression = ± 1.5 ; detection limit = 3% of total CaCO₃ measured). Dashed curves correspond to 95% confidence interval of the regression.

allowed to dry overnight. A powder XRD pattern of the prepared material was generated with a Rigaku Multiflex powder X-ray diffractometer at UNC-CH.

The %-calcite of CaCO₃ accreted by the organisms under the experimental conditions was calculated from the ratio (R) of the area under the primary calcite peak [$d(104)$; $2.98-3.03$; $2\theta = 29.5-30.2^\circ$] to the sum of the area under the primary aragonite peaks [$d(111) = 3.39$; $2\theta = 26.3^\circ$; $d(021) = 3.28$; $2\theta = 27.2^\circ$] and the primary calcite peak [$d(104) = 2.98-3.03$; $2\theta = 29.5-30.2^\circ$] (Milliman, 1974):

$$R = \frac{\text{Calcite } d(104)\text{peak}}{[\text{Aragonite } d(111)\text{peak} + \text{Aragonite } d(021)\text{peak} + \text{Calcite } d(104)\text{peak}]} \quad (1)$$

Percent-aragonite was calculated as 100% minus %-calcite.

The algorithm relating %-calcite to R (peak area ratio) was derived empirically from the analysis of gravimetrically formulated mixtures (accuracy of analytical balance = ± 0.01 mg) of reagent grade (99.9% purity) low-Mg calcite and aragonite (Fisher Scientific), yielding 0, 10, 20, 30, 40, 50, 60, 70, 80, 90, and 100% calcite (Fig. 3; Milliman, 1974). The algorithm relating %-calcite to R was determined to be:

$$\% \text{-calcite} = 69.93761R^3 - 45.49681R^2 + 75.25000R. \quad (2)$$

The standard error of the calibration regression was $\pm 1.5\%$. The precision (repeatability) of the measurement was $\pm 1.0\%$. The detection limit for the minor carbonate phase was 3% of total CaCO₃ measured, as determined from measurement of gravimetrically formulated mixtures of low-Mg calcite and aragonite (0, 1, 2, 3, 4, 5, 6, 7, 8, 9, 10, 91, 92, 93, 94, 95, 96, 97, 98, 99, and 100%) calcite.

2.9. Determination of calcite Mg/Ca (Mg/Ca_c)

The Mg/Ca_c of shell and skeletal material produced under the experimental conditions was calculated from the 2θ -shift of the primary calcite peak $d(104)$ of the powder XRD pattern (Milliman, 1974).

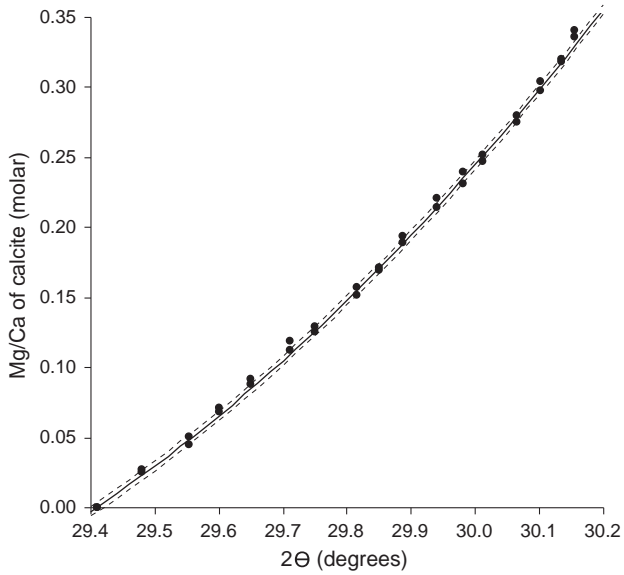


Fig. 4. Calibration curve relating calcite molar Mg/Ca to 2θ of the primary calcite peak d(104): $Mg/Ca_C = 0.17881(2\theta)^2 - 10.20926(2\theta) + 145.59368$ (standard error of regression = ±0.003). Solid circles are EDS measurements. Dashed curves correspond to 95% confidence interval of the regression.

The algorithm relating calcite-peak 2θ to Mg/Ca_C was derived empirically by X-raying calcites with Mg/Ca_C ratios ranging from 0.000 to 0.34 (independently measured via energy dispersive spectrometry (EDS) under a scanning electron microscope (Fig. 4). The equation relating Mg/Ca_C to 2θ of the primary calcite peak d(104) was determined to be:

$$Mg/Ca_C = 0.17881(2\theta)^2 - 10.20926(2\theta) + 145.59368. \quad (3)$$

The standard error of the 2θ–Mg/Ca_C calibration regression was ±0.003. The precision (repeatability) of the XRD-derived Mg/Ca_C measurement was ±0.003.

Although other methods of elemental analysis, such as secondary ion mass spectrometry, inductively coupled plasma mass spectrometry, and EDS may offer greater precision and lower detection limits than XRD for measuring Mg/Ca_C of pure, abiogenic Mg-calcite, these methods can be less accurate than XRD for measuring Mg/Ca_C of biogenic carbonates because they will also detect Mg within non-calcite phases existing within shells and skeletons (Milliman, 1974), such as brucite [Mg(OH)₂], Mg-rich organic molecules, and aragonite (Mg-poor). XRD should detect only Mg that is substituted for Ca within the calcite crystal lattice.

3. Results

3.1. Polymorph mineralogy

Powder XRD analysis (Table 3) revealed that ‘bimineralic calcifiers’ (i.e., species that produce comparable proportions of calcite and aragonite)—the calcareous serpulid worm *Hydroides crucigera* and the whelk *Urosalpinx cinerea*—produced an increasing proportion (p<0.05) of their shell as calcite with increasing pCO₂ (Fig. 5C–D). Conversely, ‘monomineralic calcifiers’ that produce >97% high-Mg calcite (the coralline red alga *Neogoniolithon* sp., the temperate urchin *Arbacia punctulata*, the tropical urchin *Eucidaris tribuloides*, the lobster *Homarus americanus*, the blue crab *Callinectes sapidus*, the shrimp *Penaeus plebejus*), >97% low-Mg calcite (the periwinkle *Littorina littorea*, the bay scallop *Argopecten irradians*, the oyster *Crassostrea virginica*, the blue mussel *Mytilus edulis*), or >97% aragonite (the hard clam *Mercenaria mercenaria*, the soft clam *Mya arenaria*, the limpet *Crepidula fornicata*, the conch *Strombus alatus*, the calcareous green alga *Halimeda incrassata*, and the temperate coral *Oculina arbuscula*) continued producing >97% of their shell/skeleton from the

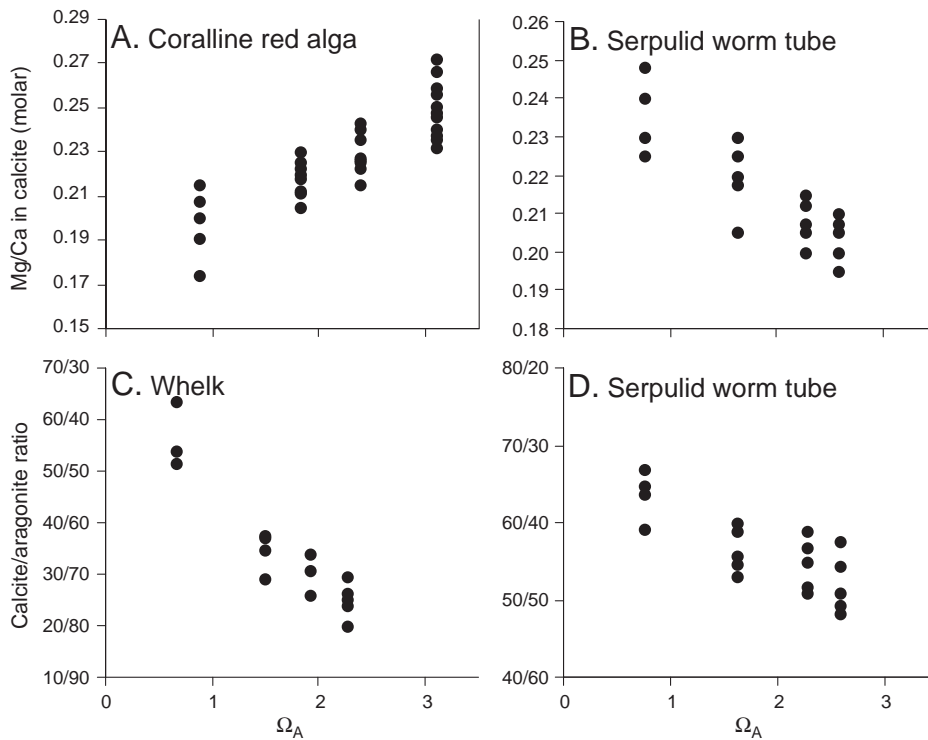


Fig. 5. Effect of CO₂-induced reductions in aragonite saturation state (Ω_A) on the calcite Mg/Ca ratio of a coralline red alga (*Neogoniolithon* sp.; A), the calcite/aragonite ratio of a whelk (*Urosalpinx cinerea*; C), and the calcite Mg/Ca ratio (B) and calcite/aragonite ratio (D) of a serpulid worm tube (*Hydroides crucigera*). Calcite/aragonite and calcite Mg/Ca ratios were determined by calibrated powder X-ray diffraction.

Table 3
Calcite Mg/Ca and calcite/aragonite ratios of shells and skeletons produced by marine calcifiers under various seawater Ω_A .

Organism	n ^a	Δ^b	Net Diss ^c	Cov ^d	mMg/Ca in calcite (\pm standard deviation)				%calcite/%aragonite (\pm standard deviation) ^g							
					$\Omega_A = 2.5$	$\Omega_A = 2.0$	$\Omega_A = 1.5$	$\Omega_A = 0.7$	R ^{2e}	p ^f	$\Omega_A = 2.5$	$\Omega_A = 2.0$	$\Omega_A = 1.5$	$\Omega_A = 0.7$	R ^{2e}	p ^f
<i>Hydroides crucigera</i> (serpulid worm)	19	—	No	Low	0.203 \pm 0.006	0.208 \pm 0.006	0.219 \pm 0.009	0.235 \pm 0.010	0.74	<0.01	50/50 \pm 5	54/46 \pm 4	56/44 \pm 4	65/35 \pm 4	0.62	<0.01
<i>Urosalpinx cinerea</i> (whelk)	15	—	Yes	Low	0.005 \pm 0.004	0.006 \pm 0.003	0.006 \pm 0.004	0.007 \pm 0.002	0.04	0.51	25/75 \pm 4	30/70 \pm 4	34/66 \pm 4	56/44 \pm 6	0.84	<0.01
<i>Neogoniolithon</i> sp. (red alga)	32	\cap	No	High	0.249 \pm 0.013	0.229 \pm 0.009	0.217 \pm 0.008	0.197 \pm 0.012	0.73	<0.01	>97% C	>97% C	>97% C	>97% C	N/A	N/A
<i>Arbacia punctulata</i> (urchin spine)	17	\cap	No	High	0.061 \pm 0.006	0.060 \pm 0.008	0.064 \pm 0.004	0.062 \pm 0.003	0.02	0.57	>97% C	>97% C	>97% C	>97% C	N/A	N/A
<i>Arbacia punctulata</i> (urchin test)	17	\cap	No	High	0.086 \pm 0.006	0.091 \pm 0.005	0.087 \pm 0.007	0.087 \pm 0.010	0.01	0.80	>97% C	>97% C	>97% C	>97% C	N/A	N/A
<i>Euclidaris tribuloides</i> (urchin spine)	22	\cap	Yes	Low	0.054 \pm 0.005	0.056 \pm 0.006	0.055 \pm 0.005	0.055 \pm 0.006	0.00	0.92	>97% C	>97% C	>97% C	>97% C	N/A	N/A
<i>Euclidaris tribuloides</i> (urchin test)	22	\cap	Yes	Low	0.124 \pm 0.003	0.122 \pm 0.002	0.123 \pm 0.003	0.123 \pm 0.004	0.01	0.61	>97% C	>97% C	>97% C	>97% C	N/A	N/A
<i>Homarus americanus</i> (lobster)	14	\cap	No	High	0.092 \pm 0.004	0.090 \pm 0.006	0.096 \pm 0.006	0.094 \pm 0.007	0.03	0.55	>97% C	>97% C	>97% C	>97% C	N/A	N/A
<i>Callinectes sapidus</i> (blue crab)	20	+	No	High	0.072 \pm 0.004	0.072 \pm 0.004	0.070 \pm 0.004	0.073 \pm 0.003	0.01	0.67	>97% C	>97% C	>97% C	>97% C	N/A	N/A
<i>Penaeus plebejus</i> (shrimp)	14	+	No	High	0.047 \pm 0.010	0.042 \pm 0.009	0.045 \pm 0.008	0.044 \pm 0.011	0.01	0.77	>97% C	>97% C	>97% C	>97% C	N/A	N/A
<i>Littorina littorea</i> (periwinkle)	19	—	No	Mod	0.003 \pm 0.002	0.004 \pm 0.002	0.003 \pm 0.002	0.003 \pm 0.002	0.01	0.69	>97% C	>97% C	>97% C	>97% C	N/A	N/A
<i>Argopecten irradians</i> (bay scallop)	20	—	No	Low	0.020 \pm 0.005	0.015 \pm 0.003	0.018 \pm 0.005	0.018 \pm 0.003	0.00	0.99	>97% C	>97% C	>97% C	>97% C	N/A	N/A
<i>Crassostrea virginica</i> (oyster)	16	—	No	Low	0.005 \pm 0.003	0.005 \pm 0.004	0.004 \pm 0.003	0.005 \pm 0.003	0.00	0.96	>97% C	>97% C	>97% C	>97% C	N/A	N/A
<i>Mytilus edulis</i> (blue mussel)	20	\emptyset	No	Mod	0.003 \pm 0.002	0.004 \pm 0.002	0.003 \pm 0.002	0.003 \pm 0.002	0.00	0.81	>97% C	>97% C	>97% C	>97% C	N/A	N/A
<i>Mercenaria mercenaria</i> (hard clam)	19	\cap	Yes	Low	N/A	N/A	N/A	N/A	N/A	N/A	>97% A	>97% A	>97% A	>97% A	N/A	N/A
<i>Mya arenaria</i> (soft clam)	11	—	Yes	Low	N/A	N/A	N/A	N/A	N/A	N/A	>97% A	>97% A	>97% A	>97% A	N/A	N/A
<i>Crepidula fornicata</i> (limpet)	18	\cap	No	Low	N/A	N/A	N/A	N/A	N/A	N/A	>97% A	>97% A	>97% A	>97% A	N/A	N/A
<i>Strombus alatus</i> (conch)	20	\cap	No	Low	N/A	N/A	N/A	N/A	N/A	N/A	>97% A	>97% A	>97% A	>97% A	N/A	N/A
<i>Halimeda incrassata</i> (green alga)	16	\cap	No	High	N/A	N/A	N/A	N/A	N/A	N/A	>97% A	>97% A	>97% A	>97% A	N/A	N/A
<i>Oculina arbuscula</i> ^h (coral)	21	\cap	No	High	N/A	N/A	N/A	N/A	N/A	N/A	>97% A	>97% A	>97% A	>97% A	N/A	N/A

(a) 'n' = number of specimens analyzed.

(b) ' Δ ' = calcification response (calcification response ('—' = negative; ' \cap ' = parabolic; ' \cap ' = threshold negative; ' \cap ' = threshold positive; '+' = positive; ' \emptyset ' = no response; Ries et al., 2009).

(c) 'Net Diss' = net dissolution (dissolution > calcification).

(d) 'Cov' = extent to which shell or skeleton is covered by an external organic layer (Ries et al., 2009).

(e) 'R²' = correlation coefficient.

(f) 'p' = p-values (bold font denotes statistically significant linear regression at the 95% confidence level or $p \leq 0.05$).

(g) >97% abundance is reported when only one CaCO₃ polymorph was identified by XRD because of the 3% detection limit of the XRD method.

(h) Data for *Oculina arbuscula* is from Ries et al. (2010).

same polymorph of CaCO₃ that they utilized under the control CO₂ treatments (Table 3).

3.2. Calcite Mg/Ca ratio

Powder XRD analysis (Table 3) revealed that Mg/Ca_C decreased ($p < 0.05$) for the coralline red alga (Fig. 5A) and increased ($p < 0.05$) for the high-Mg calcite portion of the serpulid worm tube (Fig. 5B) with increasing pCO₂. However, no statistically significant trend ($p > 0.05$) was identified between pCO₂ and Mg/Ca_C for the other high-Mg- or low-Mg-calcite-producing organisms (Table 3).

4. Discussion

4.1. Variability in biomineralogical responses amongst species

4.1.1. The role of preferential dissolution of the more soluble polymorph

One potential explanation for the increase in calcite/aragonite (C:A) ratios within the bimineralic whelk and the serpulid worm tube under conditions of elevated pCO₂ is preferential dissolution of the more soluble phases of CaCO₃ (i.e., aragonite and higher-Mg calcite; Fig. 1). However, this explanation is not consistent with the response of the serpulid worm (Fig. 5B,D), which actually increased the proportion of its high-Mg calcite phase ($0.20 < \text{Mg}/\text{Ca}_C < 0.25$) relative to its less soluble aragonite phase (Fig. 1; Andersson et al., 2008) under the more acidified conditions. The Mg/Ca_C of the calcitic portion of the worm tube also increased with increasing pCO₂ (Fig. 5B), rendering it even more soluble under the acidified conditions.

Preferential dissolution of the more soluble phase may explain the response of the whelk, which exhibited an increase in the relative abundance of its less soluble low-Mg calcite polymorph under more acidified conditions. However, if dissolution of the more soluble polymorph was responsible for the observed changes in C:A ratios within the whelk, then this response should only be realized under conditions in which the experimental seawater is undersaturated with respect to the more soluble aragonite phase ($\Omega_A < 1$; Fig. 1). Critically, the increase in C:A ratio of the whelk commenced in experimental seawaters that were supersaturated with respect to aragonite ($\Omega_A = 1.9\text{--}2.3$; Table 1; Fig. 5C).

Nevertheless, it is also possible that it was more difficult for the whelk to rid itself of metabolic acids under the CO₂-acidified treatments, which could conceivably cause its calcifying medium to become undersaturated with respect to its biomineral(s) despite its external seawater remaining supersaturated. This seems more plausible for calcifiers known to exert weak control over pH at their site of calcification, such as mollusks (Crenshaw, 1972).

4.1.2. The role of carbonate chemistry at the site of calcification

Differences in carbonate chemistry at the site of calcification may contribute to the diverse mineralogical responses exhibited by the investigated organisms. Ries et al. (2009) observed that the suite of organisms investigated in the present study exhibited highly varied responses in calcification rate to elevated pCO₂, including positive, parabolic, threshold, negative and no-response. They hypothesized that differences in pH at the organisms' sites of calcification, driven by, for example, variable proton-pumping efficiency (e.g., Al-horani et al., 2003; Ries, in press), play a critical role in modulating organisms' unique calcification response to elevated atmospheric pCO₂. For example, maintaining a high pH (e.g., 9–10) at the site of calcification would convert much of the elevated DIC resulting from elevated pCO₂, primarily in the form of HCO₃⁻, back into CO₃²⁻ for calcification. If proton regulation at the site of calcification indeed modulates some organisms' calcification responses to CO₂-induced ocean acidification by maintaining CaCO₃ saturation states above those of ambient seawater, then carbonate chemistry at the site of calcification—which would thus respond differently than that of ambient seawater to elevated

atmospheric pCO₂ (see Ries, in press)—could control calcite/aragonite and Mg/Ca_C ratios within the shells and skeletons of these organisms (Fig. 1).

There is, however, thought to be considerable variability (and uncertainty) amongst different groups of marine calcifiers as to the constitutions of their calcifying media. For example, corals (e.g., Al-Horani et al., 2003; Cohen and McConnaughey, 2003) and mollusks (e.g., Crenshaw, 1972) are thought to accrete CaCO₃ directly from a discrete calcifying fluid, with mineralization sites and crystal orientations being influenced (to vary extents) by organic templates. Calcifying bryopsidalean algae, such as Halimeda (Borowitzka and Larkum, 1976; De Beer and Larkum, 2001; Ries, 2009), are thought to precipitate their aragonite needles from a discrete calcifying fluid as well, although without the control afforded by organic crystal nucleation templates. Crustacea are also known to nucleate their shells from a discrete calcifying fluid (Cameron, 1985)—a process that must occur rapidly within these organisms as they periodically molt. Although mineralization appears to be guided by organic templates in some regions of the crustacean shell, the crystal organization process is complex and does not appear to be governed by the gross morphology of the organic matrix (Roer and Dillaman, 1984). Echinoids, on the other hand, are thought to initiate calcification on three-dimensional Ca²⁺-binding organic matrices within intracellular vacuoles (Ameje et al., 1998).

Regardless of the exact nature of the medium from which organisms produce their CaCO₃ (fluid, gels, with or without organic templates, etc.), the organism's ability to control the pH of its calcifying medium should strongly influence the medium's CaCO₃ saturation state, and thus the polymorph mineralogy and Mg-content of the biominerals that precipitate from it. Future work investigating the biomineralogical response to CO₂-induced ocean acidification should target the nature and composition of the medium from which organisms produce their shells and skeletons, as well as organisms' ability to control the composition of their calcifying media amidst variations in the chemistry of their surrounding seawater.

4.1.3. The role of utilizing amorphous calcium carbonate in the biomineralization process

There is growing evidence that many marine calcifiers produce amorphous calcium carbonate (ACC) as a precursor to their crystalline calcite and/or aragonite shells and skeletons (e.g., Addadi et al., 2003; Beniash et al., 1997; Politi et al., 2004; Roer and Dillaman, 1984; Weiner et al., 2003). The extent to which organisms utilize ACC may also play a role in their disparate and, in some cases, unexpected biomineralogical responses to elevated pCO₂. Because ACC is generally more soluble than crystalline forms of CaCO₃, organisms that utilize ACC as a precursor phase may experience the effects of elevated pCO₂ when they initially produce the ACC, rather than when that ACC stabilizes as a crystalline mineral. Furthermore, differences in the short-range ordering of ACC are thought to influence its ultimate crystalline form: aragonite, low-Mg calcite, or high-Mg calcite (Weiner et al., 2003). Although relatively little is known about how such differences in the short-range ordering of ACC affect its solubility in seawater, it is possible that the relative solubilities of ACC precursors to low-Mg calcite, high-Mg calcite, and aragonite do not mirror the relative solubilities of their crystalline end-products. Thus, the manner and extent to which organisms utilize ACC in their biomineralization process may explain, in part, the deviation of their mineralogical responses (Table 3) from those predicted from the relative solubilities of the crystalline end-products within their shells and skeletons (Fig. 1).

It should be emphasized, however, that there is considerable uncertainty over the extent to which marine calcifiers produce ACC as a precursor to their crystalline end-products. Of the various groups of calcifiers investigated here, there is evidence that crustacea (Roer and Dillaman, 1984), mollusks (cf. Weiner et al., 2003), and echinoids (Politi et al., 2004) utilize ACC as precursor phase in the construction of their shells and skeletons. A more rigorous understanding of

the extent to which marine calcifiers utilize ACC in the calcification process, and of the relative solubilities of different forms of ACC, is required to assess the hypothesis that ocean acidification acts upon this ACC precursor phase.

4.1.4. The role of calcification rate

Abiotic batch-type precipitation experiments suggest that Mg/Ca ratios within aragonite and calcite should increase with crystal growth rates (e.g., Cohen and Gaetani, 2010; Gaetani and Cohen, 2006; Watson, 2004). Yet this relationship, cannot explain changes in calcite Mg/Ca ratios that occurred within calcite produced by the serpulid worm and the coralline red alga under the investigated CO₂-induced CaCO₃ saturation states because the parabolic calcification response exhibited by the coralline red alga (Ries et al., 2009) was accompanied by an approximately linear decrease in Mg/Ca_C with increasing pCO₂ (Table 3, Fig. 5A), while the declining calcification rates for the serpulid worm (Ries et al., 2009) were accompanied by an approximately linear increase in Mg/Ca_C with increasing pCO₂ (Table 3, Fig. 5B). Assuming that whole-organism calcification rates reflect crystal growth rates, these observations are not consistent with what is predicted from the abiotic precipitation experiments and models investigating the effect of crystal growth rate on elemental partitioning in carbonates (e.g., Cohen and Gaetani, 2010; Gaetani and Cohen, 2006; Watson, 2004).

4.1.5. The role of protective organic layers

Most calcifying marine organisms cover their shells, skeletons, or tests with some type of protective organic layer, which serves to isolate their biomineral from the surrounding seawater (Ries et al., 2009; Table 3). For example, urchins cover their plates and spines with an epidermis, calcifying green and red algae precipitate CaCO₃ in extracellular spaces bound by cell walls, bivalves and gastropods cover their shells with periostracum, crustacea cover their carapaces with a thick epicuticle, and corals deposit their aragonite needles beneath several layers of epithelial tissue. By isolating shell or skeletal mineral from the external seawater, these organic coverings may prevent the more soluble phases of CaCO₃ (i.e., aragonite and higher-Mg-calcite) from dissolving in seawater that is undersaturated with respect to these minerals. Thus, this physical protection from the external seawater may influence the degree to which polymorph ratios within bimineralic calcifiers are altered by CO₂-induced ocean acidification. Notably, both species that exhibited a measurable change in C:A ratios—the serpulid worm and the whelk—cover their shells with a relatively thin organic layer.

4.2. Implications for the viability of marine calcifiers in a high-CO₂ world

4.2.1. Biomineralogical plasticity in response to CO₂-induced ocean acidification

The present experiments reveal that of the 14 investigated species that produce the more soluble aragonite and/or high-Mg calcite forms of CaCO₃ under normal pCO₂ (~409 ppm), only two will reduce the solubility of their shell/skeleton under high-CO₂ conditions by accreting a greater proportion of their shell/skeleton as low-Mg calcite (whelk; Table 3; Fig. 5C) or by reducing the Mg/Ca of the calcitic portion of their shell (coralline red alga; Table 3; Fig. 5A). Eleven of these 14 species exhibited no significant (p<0.05) change in skeletal mineralogy and one species, the calcareous serpulid worm, actually began producing a greater proportion of its shell as the more soluble high-Mg calcite polymorph, and even increased the Mg/Ca of this calcite under elevated pCO₂ (Table 3; Fig. 5B,D). These observations suggest that most benthic marine calcifiers that produce high-Mg calcite and/or aragonite shells or skeletons will not plastically adapt to CO₂-induced ocean acidification by producing less soluble forms of CaCO₃ (i.e., lower-Mg calcite instead of higher-Mg calcite or aragonite).

4.2.2. Impacts on shell/skeletal biomechanics

Marine invertebrates are thought to have evolved calcareous shells and skeletons, at least in part, to protect themselves from the crushing jaws and claws of predators (e.g., Vermeij, 1989). Shells/skeletons constructed from heterogeneous materials, such as interlaminated aragonite and calcite (Li et al., 2004; Tanur et al., 2010) and even high-Mg calcite (due to size differences between the Mg²⁺ and Ca²⁺ cations in the calcite crystal lattice; Magdams and Gies, 2004), have been shown to exhibit unique biomechanical properties—including enhanced resistance to crack propagation. Thus, the biomechanical properties of the shells of the three species investigated in the present study whose mineralogy did change under conditions of elevated pCO₂ (i.e., the whelk, serpulid worm, and coralline red alga) may be altered by these mineralogical changes, potentially exacerbating the impact of reduced calcification rates exhibited by these species under high pCO₂ conditions (Ries et al., 2009). The biomechanical impacts of altering the ratios of CaCO₃ polymorphs within bimineralic calcifiers, Mg/Ca ratios within calcite-producing organisms, and the density and ultrastructure of shell/skeletal materials are presently being assessed by the author.

4.2.3. Does mineralogical plasticity confer resilience to seawater acidification?

The extent to which mineralogical plasticity enables organisms to maintain calcification rates (Ries et al., 2009) in CO₂-acidified seawater is not clear-cut (Table 3). Organisms that exhibited no change in mineralogy under the acidified conditions exhibited the full suite of calcification rate responses: positive, threshold positive, parabolic (positive under moderate acidification, negative under extreme), threshold negative, and negative (Table 3; Ries et al., 2009). Likewise, the three species that did exhibit a plastic mineralogical response to the acidified conditions—the coralline red alga (decrease in Mg/Ca_C), the serpulid worm (increase in C:A ratio, increase in Mg/Ca_C), and the whelk (increase in C:A ratio)—exhibited both parabolic (coralline red alga) and negative (serpulid worm, whelk) calcification rate responses to the acidified treatments (Table 3, Ries et al., 2009). Thus, both positive/parabolic and negative calcification rate responses to CO₂-induced acidification were exhibited by organisms that demonstrated mineralogical plasticity, as well as those that did not.

4.3. Implications for the calcite–aragonite seas hypothesis

A large body of research has been dedicated to investigating whether secular trends in the polymorph mineralogy of marine carbonates throughout Phanerozoic time, so-called 'calcite-and-aragonite seas' (reviewed by Ries, 2010), were driven primarily by atmospheric pCO₂ (e.g., Zhuravlev and Wood, 2009) or by seawater Mg/Ca (e.g., Hardie, 1996) which are thought to vary approximately inversely with one another, as they both appear to be largely controlled by the global rate of ocean crust production (see Ries, 2010). The results of the present study suggest that some bimineralic calcifiers, such as whelks (Fig. 5C) and calcareous serpulid worms (Fig. 5D), may have produced a greater proportion of their shell as the calcite polymorph under conditions of elevated pCO₂. Indeed, both Railsback (1993) and Vinn and Mutvei (2009) showed that calcite/aragonite ratios within calcareous serpulid worm tubes have varied in general synchrony with seawater Mg/Ca throughout Phanerozoic time. The results presented here suggest that this trend may have been driven, at least in part, by concomitant fluctuations in atmospheric pCO₂ and seawater CaCO₃ saturation state (e.g., Zhuravlev and Wood, 2009).

4.4. Implications for paleoceanographic reconstructions

Calcite Mg/Ca within Mg-calcite marine organisms (e.g., echinoids, coralline red algae) has been interpreted as a proxy of seawater Mg/

Ca, temperature, and salinity (e.g., Borremans et al., 2009; Dickson, 2004; Halfar et al., 2000; Kamenos et al., 2008). The observation that Mg/Ca_C within the skeletons of calcareous serpulid worms and coralline red algae is influenced by the carbonate chemistry of seawater suggests that well-preserved fossils of these organisms—and possibly others—may also contain information about paleo-atmospheric pCO₂ and CaCO₃ saturation states of the ancient ocean. However, this application may be limited by the fact that changes in Mg/Ca_C driven by geologically realistic changes in seawater Ω_A are small compared with changes in Mg/Ca_C driven by other physico-chemical parameters of seawater that have changed throughout geologic time (see Ries, 2010). For instance, geologically realistic changes in seawater Ω_A (~0.7–3) only caused Mg/Ca_C to vary by about 4 percentage points (0.21–0.25) within the coralline red algae and the serpulid worm tubes. In contrast, geologically realistic changes in seawater temperature (0–30 °C) caused Mg/Ca_C to vary by 25 percentage points in coralline red algae (0.08–0.33; Chave, 1954) and by about 14 percentage points in serpulid worms (0.08–0.22; Chave, 1954). Likewise, geologically realistic changes in seawater molar Mg/Ca (1–5) caused Mg/Ca_C to vary by about 20 percentage points in coralline red algae (0.06–0.26; Ries, 2006) and by about 16 percentage points in serpulid worms (0.03–0.19; Ries, 2004). Nevertheless, reconstructions of seawater Mg/Ca and temperature—which appear to exert stronger control on skeletal Mg/Ca_C than does seawater Ω_A—may be improved by controlling for the effects of paleo-seawater Ω_A on shell/skeletal Mg-fractionation.

5. Conclusion

These experiments reveal that CO₂-induced reductions in seawater Ω_A from 2.5 ± 0.4 to 0.7 ± 0.2 do not substantially alter the polymorph mineralogy of monomineralic marine calcifiers, although they do cause an increase in C:A ratios within some bimineralic marine calcifiers. The CO₂-induced reductions in seawater Ω did not influence Mg/Ca_C within most of the Mg-calcite-producing species, but did cause a decrease in Mg/Ca_C within the coralline red alga and an increase within the serpulid worm tube, suggesting that paleoceanographic reconstructions based on Mg/Ca_C of these organisms may be improved by accounting for the effects of seawater Ω. Various factors may be responsible for the disparate mineralogical responses to CO₂-induced ocean acidification that were observed amongst the investigated taxa. Future work should focus on the roles that species-specific differences in carbonate chemistry at the site of calcification and the use of amorphous CaCO₃ as a precursor to crystalline CaCO₃ play in driving these varied mineralogical responses to CO₂-induced ocean acidification.

Acknowledgments

The author extends gratitude to A. Cohen and D. McCorkle. This research was supported by a WHOI Ocean and Climate Change Postdoctoral Fellowship, funding from the WHOI Tropical Research Institute, NSF awards #1031995 (to Ries) and #0648157 (to Cohen & McCorkle), and a UNC faculty development grant. The funding agencies played no role in the study design; in the collection, analysis and interpretation of data; in the writing of the manuscript; or in the decision to submit the paper for publication. [SS]

References

- Addadi, L., Raz, S., Weiner, S., 2003. Taking advantage of disorder: amorphous calcium carbonate and its roles in biomineralization. *Advanced Materials* 15, 959–970.
- Al-Horani, F.A., Al-Moghrabi, S.M., DeBeer, D., 2003. The mechanism of calcification and its relation to photosynthesis and respiration in the scleractinian coral *Galaxea fascicularis*. *Marine Biology* 142, 419–426.
- Ameys, L., Compere, P., Dille, J., Dubois, P., 1998. Ultrastructure and cytochemistry of the early calcification site and of its mineralization organic matrix in *Paracentrotus lividus* (Echinodermata: Echinoidea). *Histochemistry and Cellular Biology* 110, 285–294.
- Andersson, A.J., Mackenzie, F.T., Bates, N.R., 2008. Life on the margin: implications of ocean acidification on Mg-calcite, high latitude and cold-water marine calcifiers. *Marine Ecology Progress Series* 373, 265–273.
- Beniash, E., Aizenberg, J., Addadi, L., Weiner, S., 1997. Amorphous calcium carbonate transforms into calcite during sea urchin larval spicule growth. *Proceedings of the Royal Society of London* 264, 461–465.
- Bischoff, W.D., Bishop, F.C., Mackenzie, F.T., 1983. Biogenically produced magnesian calcite: inhomogeneities in chemical and physical properties: comparison with synthetic phases. *American Mineralogist* 68, 1183–1188.
- Borowitzka, M.A., Larkum, A.W.D., 1976. Calcification in the green alga *Halimeda*. III. The sources of inorganic carbon for photosynthesis and calcification and a model of the mechanism of calcification. *Journal of Experimental Biology* 27, 879–893.
- Borremans, C., Hermans, J., Baillon, S., André, L., Dubois, P., 2009. Salinity effects on the Mg/Ca and Sr/Ca in starfish skeletons and the echinoderm relevance for paleoenvironmental reconstructions. *Geology* 37, 351–354.
- Bradshaw, A.L., Brewer, P.G., Shafer, D.K., Williams, R.T., 1981. Measurements of total carbon dioxide and alkalinity by potentiometric titration in the GEOSECS program. *Earth and Planetary Science Letters* 55, 99–115.
- Brewer, P.G., 1997. Ocean chemistry of the fossil fuel CO₂ signal: the haline signal of “business as usual”. *Geophysical Research Letters* 24, 1367–1369.
- Cameron, J.N., 1985. Post-moult calcification in the blue crab (*Callinectes sapidus*): Relationships between apparent net H⁺ excretion, calcium and bicarbonate. *The Journal of Experimental Biology* 119, 275–285.
- Chave, K.E., 1954. Aspects of the Biogeochemistry of magnesium, 1. Calcareous marine organisms. *Journal of Geology* 62, 266–283.
- Cohen, A.L., Gaetani, G.A., 2010. Ion partitioning and the geochemistry of coral skeletons: solving the mystery of the vital effect. *European Mineralogical Union Notes in Mineralogy* 11, 377–397.
- Cohen, A.L., McConnaughey, T.A., 2003. A geochemical perspective on coral mineralization. In: Dove, P.M., Weiner, S., De Yoreo, J.J. (Eds.), *Biomineralization: reviews in mineralogy and geochemistry*, v. 54. American Geological Institute, Washington D.C., pp. 151–187.
- Crenshaw, M.A., 1972. The inorganic composition of molluscan extrapallial fluid. *The Biological Bulletin* 143, 506–512.
- De Beer, D., Larkum, A.W.D., 2001. Photosynthesis and calcification in the calcifying alga *Halimeda discoidea* studied with microsensors. *Plant, Cell & Environment* 24, 1209–1217.
- de Choudens-Sanchez, V., Gonzalez, L., 2009. Calcite and aragonite precipitation under controlled instantaneous supersaturation: elucidating the role of CaCO₃ saturation state and Mg/Ca ratio on calcium carbonate polymorphism. *Journal of Sedimentary Research* 79, 363–376.
- Dickson, J.A.D., 2004. Echinoderm skeletal preservation: calcite–aragonite seas and the Mg/Ca ratio of Phanerozoic oceans. *Journal of Sedimentary Research* 74, 355–365.
- Feely, R.A., Sabine, C.L., Hernandez-Ayon, J.M., Janson, D., Hales, B., 2008. Evidence for upwelling of corrosive “acidified” water onto the continental shelf. *Science* 320, 1490–1492.
- Gaetani, G.A., Cohen, A.L., 2006. Element partitioning during precipitation of aragonite from seawater: a framework for understanding paleoproxies. *Geochimica et Cosmochimica Acta* 70, 4617–4634.
- Halfar, J., Zack, T., Kronz, A., Zachos, J.C., 2000. Growth and high-resolution paleoenvironmental signals rhodoliths (coralline red algae): a new biogenic archive. *Journal of Geophysical Research* 105, 22107–22116.
- Hardie, L.A., 1996. Secular variation in seawater chemistry: an explanation for the coupled secular variation in the mineralogies of marine limestones and potash evaporites over the past 600 m.y. *Geology* 24, 279–283.
- Kamenos, N.A., Cusack, M., Moore, P.G., 2008. Coralline algae are global paleothermometers with bi-weekly resolution. *Geochimica et Cosmochimica Acta* 72, 771–779.
- Lee, J., Morse, J.W., 2010. Influences of alkalinity and pCO₂ on CaCO₃ nucleation from estimated Cretaceous composition seawater representative of “calcite seas”. *Geology* 38, 115–118.
- Li, X., Chang, W., Chao, Y.J., Wang, R., Chang, M., 2004. Nanoscale structural and mechanical characterization of a natural nanocomposite material: the shell of the red abalone. *Nano Letters* 4, 613–617.
- Lowenstam, H.A., 1954. Factors affecting the aragonite: calcite ratios in carbonate-secreting marine organisms. *Journal of Geology* 62, 284–322.
- Magdams, U., Gies, H., 2004. Single crystal structure of sea urchin spine calcites: Systematic investigations of the Ca/Mg distribution as a function of habitat of the sea urchin and the sample location in the spine. *European Journal of Mineralogy* 16, 261–268.
- Milliman, J.D., 1974. *Marine carbonates*. Springer-Verlag, Berlin.
- Mucci, A., 1983. The solubility of calcite and aragonite in seawater at various salinities, temperatures, and one atmosphere total pressure. *American Journal of Science* 283, 780–799.
- National Oceanic and Atmospheric Administration, 2008. National Oceanic and Atmospheric Administration Integrated Ocean Observing System. <http://ioos.noaa.gov/program/products.html>.
- Pierrot, D., Lewis, E., Wallace, D.W.R., 2006. MS Excel Program Developed for CO₂ System Calculations. ORNL/CDIAC-105a. Carbon Dioxide Information Analysis Center, Oak Ridge National Laboratory, U.S. Department of Energy, Oak Ridge, Tennessee.
- Politi, Y., Arad, T., Klein, E., Weiner, S., Addadi, L., 2004. Sea urchin spine calcite forms via a transient amorphous calcium carbonate phase. *Science* 306, 1161–1164.
- Railsback, L.B., 1993. Original mineralogy of carboniferous worm tubes—evidence for changing marine chemistry and biomineralization. *Geology* 21, 703–706.

- Ries, J.B., 2004. The effect of ambient Mg/Ca on Mg fractionation in calcareous marine invertebrates: a record of Phanerozoic Mg/Ca in seawater. *Geology* 32, 981–984.
- Ries, J.B., 2006. Mg fractionation in crustose coralline algae: Geochemical, biological, and sedimentological implications of secular variation in the Mg/Ca ratio of seawater. *Geochimica et Cosmochimica Acta* 70, 891–900.
- Ries, J.B., 2009. Effects of secular variation in seawater Mg/Ca ratio (calcite–aragonite seas) on CaCO₃ sediment production by the calcareous algae *Halimeda*, *Penicillus* and *Udotea*—evidence from recent experiments and the geological record. *Terra Nova* 21, 323–339.
- Ries, J.B., 2010. Geological and experimental evidence for secular variation in seawater Mg/Ca (calcite–aragonite seas) and its effects on marine biological calcification. *Biogeosciences* 7, 2795–2849.
- Ries, J.B., in press. A Physicochemical framework for interpreting the biological calcification response to CO₂-induced ocean acidification, *Geochimica et Cosmochimica Acta*.
- Ries, J.B., Cohen, A.L., McCorkle, D.C., 2009. Marine calcifiers exhibit mixed responses to CO₂-induced ocean acidification. *Geology* 37, 1131–1134.
- Ries, J.B., Cohen, A.L., McCorkle, D.C., 2010. A nonlinear calcification response to CO₂-induced ocean acidification by the temperate coral *Oculina arbuscula*. *Coral Reefs* 29, 661–674.
- Roer, R., Dillaman, R., 1984. The structure and calcification of the crustacean cuticle. *Integrative and Comparative Biology* 24, 893–909.
- Rogers, W.H., 1993. Regression standard errors in clustered samples. *Stata Technical Bulletin* 13, 19–23.
- Roy, R.N., Roy, L.N., Vogel, K.M., Porter-Moore, C., Pearson, T., Good, C.E., Millero, F.J., Campbell, D.M., 1993. The dissociation constants of carbonic acid in seawater at salinities 5 to 45 and temperatures 0 to 45 °C. *Marine Chemistry* 44, 249–267.
- Tanur, A.E., Gunari, N., Sullan, R.M.A., Kavanagh, C.J., Walker, G.C., 2010. Insights into the composition, morphology, and formation of the calcareous shell of the serpulid *Hydroides dianthus*. *Journal of Structural Biology* 169, 145–160.
- Vermeij, G., 1989. The origin of skeletons. *Palaos* 4, 585–589.
- Vinn, O., Mutvei, H., 2009. Calcareous tubeworms of the Phanerozoic. *Estonian Journal of Earth Sciences* 58, 286–296.
- Watson, E.B., 2004. A conceptual model for near-surface kinetic controls on the trace-element and stable isotope composition of abiogenic calcite crystals. *Geochimica et Cosmochimica Acta* 7, 1473–1488.
- Weiner, S., Levi-Kalisman, Y., Raz, S., Addadi, L., 2003. Biologically formed amorphous calcium carbonate. *Connective Tissue Research* 44, 214–218.
- Zhuravlev, A.Y., Wood, R.A., 2009. Controls on carbonate skeletal mineralogy: Global CO₂ evolution and mass extinctions. *Geology* 37, 1123–1126.